

When there is a discrepancy between the information in this technical report and information in JDox, assume JDox is correct.



**STScI** | SPACE TELESCOPE  
SCIENCE INSTITUTE

## JWST TECHNICAL REPORT

Title: NIRSpec Sensitivity Monitor Observations: Description and Analysis of Cycle 1 and 2 Data	Doc #: JWST-STScI-009204, SM-12 Date: 17 November 2025 Revision -
Authors: C. R. Proffitt, C. Hayes, P. Zeidler, E. Frazer, A. Fullerton, J. Muzzerolle Phone: 301-661-1652 Page	Release Date: 8 December 2025

### 1 Abstract

We report on the stability of the NIRSpec spectroscopic throughput during the first two cycles of JWST operation. The most frequent comparisons were done as part of the cross instrument absolute flux repeatability programs, (PIDs 1539, 4499, and 6607) using the S1600A1 fixed slit aperture to take repeated G140H/F100LP observations of the A star standard BD +60 1753. Here we consider 16 epochs covering the period from March 2023 to August 2024. We also discuss repeated NIRSpec observations of the solar analogue GSPC P330-E (PIDs 1538, 4498) taken at two different epochs, (Aug 2022 and May/June 2024), as well as some more limited data for P330-E taken in August 2024 as part of the Cycle 3 program PID 6606. The P330-E observations use all NIRSpec disperser and filter combinations in the S1600A1 aperture, as well as a more limited number of settings with the NIRSpec integral field unit (IFU).

This report focuses on relative stability rather than the absolute accuracy of the flux calibration. When using exactly the same exposure setups and exposure times, the BD +60 1753 observations suggest that the typical fixed slit repeatability over broad wavelength bands with the NIRSpec gratings was as good as 0.2% during the period considered. At the level of individual pixels, the rms variability is of order 1% or less. At intermediate scales, there is little evidence for changes of more than  $\sim 0.5\%$ .

We also review results for a few flux standards that have been observed more than once with the PRISM in the S1600A1, and these can show rather larger 1 – 2% variability, especially at the shortest wavelengths. This may in part be due to higher sensitivity of the PRISM calibration to small pointing or grating alignment errors.

For the NIRSpec IFU, the limited data considered here suggests repeatability with the NIRSpec gratings is about 1%, but analysis of more recent data with better matched positioning may improve on this result.

## 2 Introduction

We discuss here NIRSpec observations suitable for testing the flux stability and repeatability of the instrument. We will emphasize data where the same target is repeatedly observed with the exact same exposure parameters and aperture positioning. Such comparisons test the stability of the optical and detector throughput and of the target alignment after the target acquisition, but do not necessarily speak to the absolute accuracy of the flux calibration, or to the relative flux consistency between non-identical observations of the same target. While most users will of course be primarily concerned about the absolute accuracy, understanding the relative stability is important for determining the ultimate limits to the accuracy, for prioritizing work on the various reference files that can limit the absolute accuracy achieved, and for science cases where changes between observations are the limiting factor.

For this report we will confine our analysis to data collected between August of 2022 and August of 2024. This covers the bulk of the first two cycles of JWST science operations. For the primary analyses, we focus on data from the Cycle 1 and 2 calibration programs 1538, 1539, 4498, and 4499, but we also include data from the first visits of the Cycle 3 programs 6606 and 6607 obtained in August 2024. We also consider some individual PRISM observations from a few other programs (1128, 1487, 1536, 1537, 4460, and 4496).

The plan for the cross-instrument flux calibration of JWST is described in Gordon et al. (2022). Part 3 of that plan is intended to monitor the stability over time by making repeated measurements with each instrument of the same target in the same mode. For NIRSpec, the selected monitor target is the star BD+60 1753 (A1V,  $K_s = 9.64$ ), and we use 17 observations of this target taken during Cycles 1 and 2 using the G140H/F100LP setting with a 5-point dither in the S1600A1 aperture. This data will be discussed in section 3.1.

We use some additional observations taken in other parts of the Gordon et al. plan to perform more limited repeatability checks for a wider variety of settings. These include repeated observations of the solar analog GSPC P330-E, (G0V,  $K_s=11.42$ ) in the S1600A1 with all the NIRSpec disperser/filter combinations, (section 3.2.1), and with a more limited number of settings with the NIRSpec integral field unit, (section 3.2.3). In section 3.2.2 we will also compare PRISM observations of standard stars that were observed more than once in the S1600A1 during the period under consideration.

## 3 Observations and Results

### 3.1 NIRSpec monitoring observations of BD+60 1753.

The JWST cross instrument sensitivity monitoring program for Cycle 1 was implemented in PID 1539 and in PIDs 4499 and 6607 for Cycles 2 and 3. The same target, BD+60 1753 was used for the monitoring of NIRCам and NIRISS modes, as well as for MIRI imaging modes. Observations were done approximately once per month.

The NIRSpec monitoring observations of this star use the G140H/F100LP in the S1600A1 with the standard 5-point dither pattern and the SUB2048 subarray. This setting was chosen as it provides coverage of both detectors in the minimum observation time. At each dither position, a single integration of 10 NRSRAPID groups is taken, giving an effective exposure time of 9.942 s per dither. The exposure setup was chosen to give  $S/N > 200$  at all wavelengths.

**Table 1: Monitoring observations of BD+60 1753 used for this analysis. For each exposure, we list the observation date as both a calendar date and a modified Julian day number, the mean flux on each detector relative to the average spectrum, and the standard deviation of the individual pixels around that mean. For these statistics, pixels deviating more than  $5\sigma$  from the mean spectrum were excluded.**

PID – Obs. Num.	OBS-DATE	MJD	Mean NRS1 0.995 – 1.31 $\mu\text{m}$	$\sigma$ (NRS1) per pixel	Mean NRS2 1.355 – 1.81 $\mu\text{m}$	$\sigma$ (NRS2) per pixel
jw01539-o041	2023-03-10	60013	1.00435	0.010	1.00118	0.008
jw01539-o046	2023-04-06	60041	0.99487	0.007	0.99531	0.006
jw01539-o051	2023-05-03	60067	1.00156	0.009	1.00145	0.006
jw01539-o056	2023-05-30	60095	1.00103	0.009	1.00197	0.006
jw01539-o061	2023-06-30	60125	1.00096	0.010	1.00283	0.007
jw04499-o003	2023-07-06	60132	1.00177	0.009	1.00204	0.006
jw04499-o010	2023-07-30	60155	0.99898	0.008	1.00024	0.006
jw04499-o017	2023-09-05	60192	1.00096	0.008	1.00172	0.006
jw04499-o024	2023-09-26	60213	1.00271	0.009	1.00484	0.007
jw04499-o031	2024-01-10	60320	1.00131	0.010	1.00148	0.007
jw04499-o038	2024-02-07	60348	0.99848	0.012	0.99674	0.010
jw04499-o045	2024-03-03	60373	0.99758	0.012	0.99737	0.008
jw04499-o052	2024-03-31	60400	1.00011	0.007	1.00028	0.006
jw04499-o059	2024-04-28	60429	1.00139	0.008	1.00082	0.006
jw04499-o066	2024-05-26	60456	1.00004	0.008	1.00010	0.006
jw04499-o073	2024-06-23	60484	0.99974	0.008	0.99964	0.006
jw06607-o006	2024-07-26	60518	1.00124	0.009	0.99884	0.006

Because of an APT error in the proper motion of the offset acquisition target, the initial visits of PID 1539 were very poorly centered in the aperture, and for this report we only consider data taken after this issue was corrected. For a full list of exposures considered here, see Table 1. Starting in Cycle 3, observations with the G235H/F170LP, (20 groups or 18.964s per dither), and G395H/F290LP, (52 groups or 47.82s per dither), have been added to each NIRSpec monitoring visit to extend the coverage to longer wavelengths, while for Cycle 4 the G140M/F070LP setting will also be added to provide coverage down to 0.7 microns. Due to the limited amount of data collected to date in these other settings, detailed discussion of these additional observations of BD+60 1753 will be deferred to a later report.

### 3.1.1 Description of data analysis

For the analysis here, the data were reduced using the JWST Science Calibration Pipeline Version 1.17.1<sup>1</sup>, and the context `jwst_1322.pmap`. We started our analysis with the standard level 1 rate files but made a few modifications to the default level 2 and 3 processing.

Since this is a bright star, the contribution of the background will be negligible. ETC calculations for G140H/F100LP observations of this target in the S1600A1 show that even the 90th percentile level for the background counts is never more than a few  $\times 10^{-5}$  of the source counts. As a result, any in aperture “background” measured in the S1600A1 will be dominated by light from the point source itself and simply provide an additional source of noise. So, we performed the level 2 processing for this target without including any background members in the association files. Because of the centering issues discussed below, (see appendix A), we constructed the level 3 s2d image using the middle three nods only, as the outer dither positions may show some variable vignetting from the aperture edge, and the lowest dither position is clearly corrupted by significant resampling artifacts at the edge of the rectified area.

As discussed below in the Appendix, for the BD+60 1753 observations, the location of the spectrum in the cross-dispersion direction of the S1600A1 aperture is shifted significantly from the location found for similarly constructed exposures that use a direct target acquisition, and there was significant variability in the position among these visits. This does not appear to be a simple error in the coordinates or proper motion of the science target or the offset star, as such an error would produce a fixed offset in RA and Dec, and the offset would change magnitude and even its sign in the telescope frame as a function of roll angle. Instead, the target always falls low in NIRSpec detector coordinates, and we find a mean offset of  $-1.134 \pm 0.487$  pixels from the expected cross-dispersion position. Given this significant offset and variability in the cross-dispersion location, we also checked for offsets in the dispersion direction by cross-correlating a rotationally broadened version of the CALSPEC<sup>2</sup> spectral model `bd60d1753_mod_006.fits` for this star, (which assumes a radial velocity of  $-27.3$  km/s), to find the shifts in the dispersion direction. However, note that we cannot distinguish between small spatial offsets in the aperture along the dispersion direction and actual velocity variations of the target. Nonetheless, for the radial velocity adopted by the CALSPEC spectrum, we found a mean offset of  $6.18 \pm 15.34$  km/s which is equivalent to  $+0.147 \pm 0.365$  pixels in the dispersion direction. Further details are given in the appendix below. The XOFFSET keywords in the rate files were adjusted to correct for the measured dispersion shift and the level 2 and 3 products were then recreated. This ensures that the wavelength scales of the different exposures are aligned when comparing the fluxes.

For the final extractions, the  $y$  center location of the spectrum in the final rectified level 3 s2d spectral image was measured by fitting a Gaussian function to each column and taking the median of all the individual center values found as the adopted spectrum center. The pipeline `Extract1dStep` was then called using a version of the `extract1d` reference file that was set up to use the “`src_coeff`” option<sup>3</sup> (see Figure 1 for an example of the syntax). The coefficients defining the upper and lower bounds of the extraction region were set to be the measured center location plus and minus half the extraction width, which for S1600A1 fixed slit spectra is 5 pixels. No higher order source coefficients were defined in the extraction table, so this same center location and

---

<sup>1</sup> See <https://jwst-pipeline.readthedocs.io/en/latest/jwst/changes.html#id116>

<sup>2</sup> <https://www.stsci.edu/hst/instrumentation/reference-data-for-calibration-and-tools/astronomical-catalogs/calspec>

<sup>3</sup> See [https://jwst-pipeline.readthedocs.io/en/latest/jwst/extract\\_1d/description.html#extract-1d-for-slits](https://jwst-pipeline.readthedocs.io/en/latest/jwst/extract_1d/description.html#extract-1d-for-slits)

width was adopted at all wavelengths. No background coefficients were defined, so no background subtraction was performed during the extraction step either.

```
{
  "id": "S1600A1",
  "region_type": "target",
  "bkg_order": 0,
  "bkg_fit": "median",
  "dispaxis": 1,
  "extract_width": 5,
  "smoothing_length": 3,
  "src_coeff": [
    [
      10.769676842771752
    ],
    [
      15.769676842771752
    ]
  ]
}
```

**Figure 1: Sample row for an extract1d reference table using src\_coeff.**

### 3.1.2 Variability Results for Sensitivity Monitor Target

To measure the observation-to-observation variability and to look for any systematic changes in the throughput over time, we start by computing an “average” spectrum to act as a reference. We do this by interpolating each individual F100LP/G140H spectrum to the wavelength scale of the first exposure<sup>4</sup>, and then find the mean value of all the spectra at each wavelength after using the `astropy.stats.sigma_clipped_stats` routine with a 5 sigma rejection threshold to remove outliers. Figure 2 shows the resulting mean spectrum. We also overplot all of the individual spectra there. While they cannot easily be distinguished from each other in this figure, they do illustrate the scale of the scatter around the mean.

---

<sup>4</sup> Note that due to the non-repeatability of the exact grating wheel position, each observations has a well-calibrated, yet slightly different wavelength zeropoint

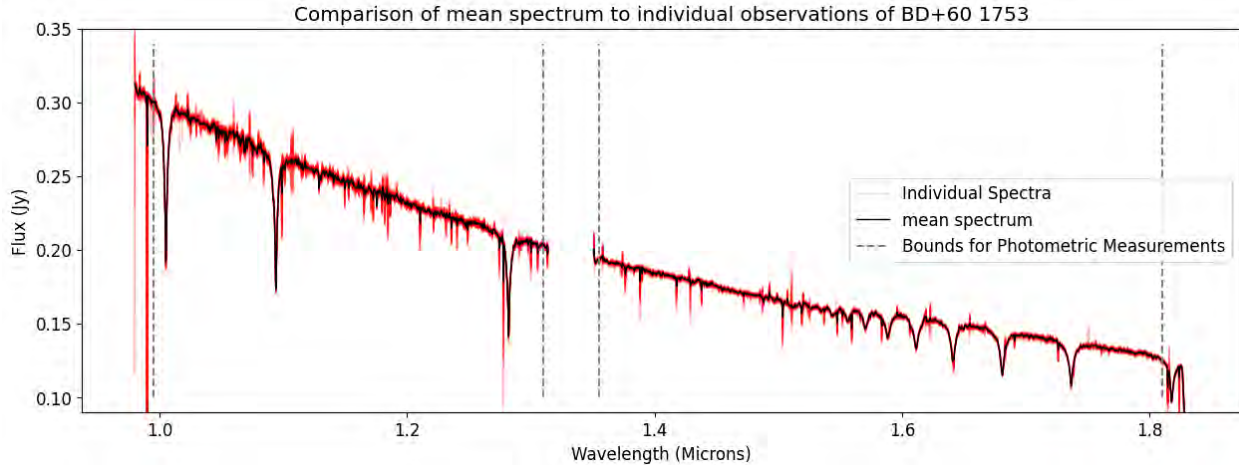


**Figure 2:** The black line shows the mean spectrum derived from the 17 observations of BD+60 1753 considered in this analysis, while the fainter red lines overplot all of the individual spectral extractions. While the individual spectra cannot be distinguished here, it does illustrate the overall consistency of the spectra.

To provide a more quantitative metric, we define one wide band to cover most of the spectrum that falls on each detector, excluding only narrow regions near the edges. These chosen boundaries are marked in Figure 2 and cover 0.995 to 1.31 microns for NRS1 and 1.355 to 1.81 microns for NRS2. The average spectrum is then interpolated back to the wavelength scale of each individual observation, so that the pixel-by-pixel ratio of each observation to the average can be computed without having to further smooth the individual observations. We then simply calculate the mean of this ratio for all pixels falling in the band. The only outlier clipping done when computing this mean is to reject a few pixels which consistently fall low, (flux less than 0.07 Jy). Figure 3 shows these resulting measured flux ratios as a function of time.

For these broad bands, the scatter of the individual values about the linear trend is about 0.2%, and any trend with time is small;  $-0.05\%/year$  for NRS1 and  $-0.12\%/year$  for NRS2 with estimated errors for the slopes of 0.12 and 0.13%/year.

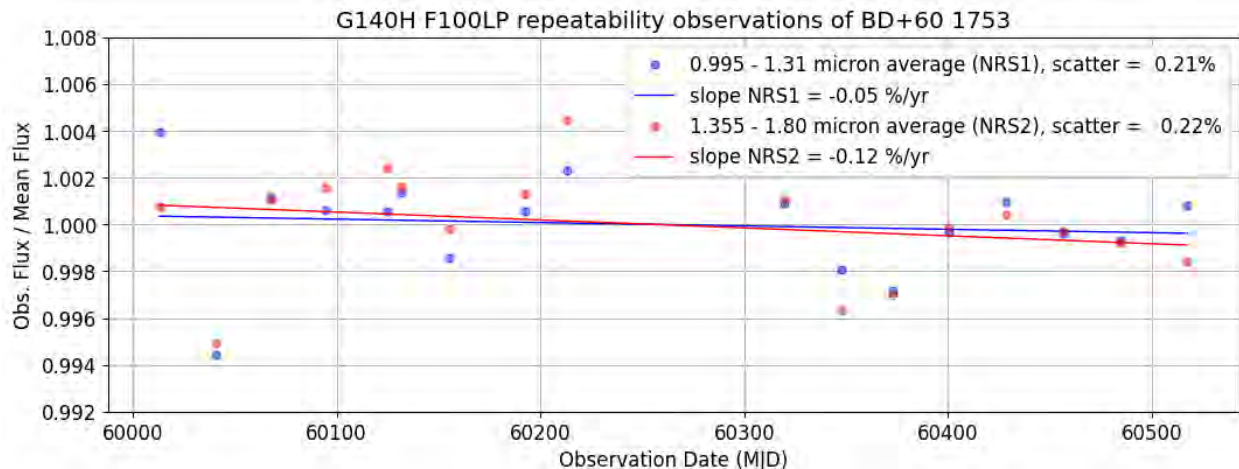


**Figure 3:** The time dependence of the ratio of the flux measured in each observation to the mean flux measured in the full set of observation is shown for two wide bands that cover most of each detector. Linear fits vs time to these measurements are also shown.

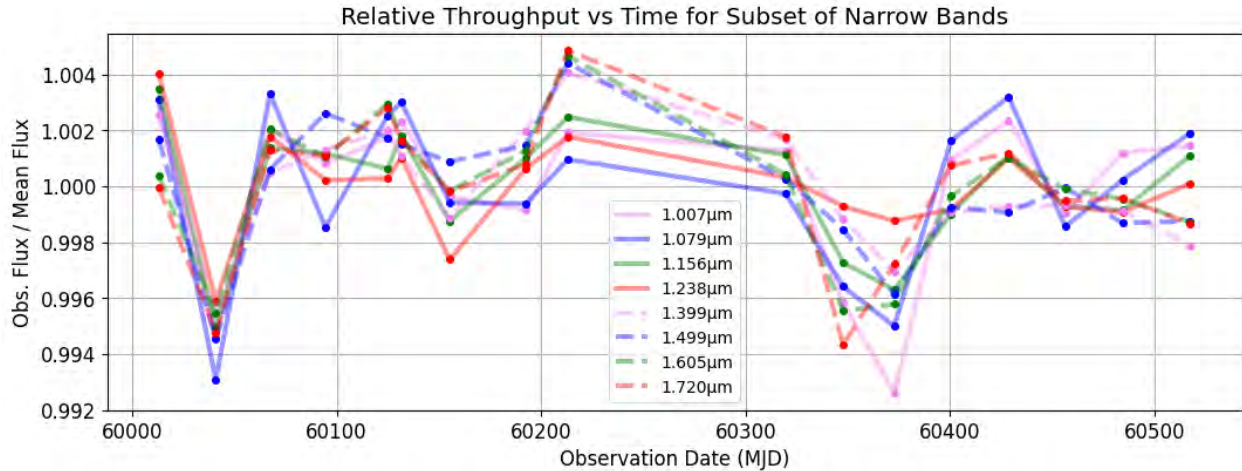


**Figure 4:** The ratios of the measured flux to the mean flux vs time for four narrow bands on each detector are shown. Solid lines are for bands on NRS1, and dashed lines for NRS2. Line colors, (violet, blue, green, red), are ordered by increasing wavelength on each detector.

If we split the wavelength range for each detector into 8 separate bands with width  $\Delta\lambda/\lambda \approx 0.034$ , and measure the slope and scatter for the flux vs time in each, we get similar if rather noisier results for the slopes as we did for the wide bands. In Figure 4, we plot the measured flux ratios vs time for 4 of these bands on each detector. For the most part the changes are strongly correlated across bands, although there are occasionally small offsets between the two detectors.

If we instead look at the error distribution for individual pixels about the value of the mean spectrum at each wavelength the typical scatter is around 1%. To illustrate typical fluctuations on small wavelength scales, we show in Figure 5, for the four observations taken between 10-Jan-2024 and 31-Mar-2024, (MJD 60319.7 to 60400.5), the detailed pixel-by-pixel ratios with respect to the mean spectrum. These dates span the apparent 0.3% dip in throughput centered at about MJD 30360 that is visible in Figure 3 and Figure 4.

The very small changes found here suggest that both the JWST + NIRSpec optical path and the NIRSpec detectors have *extraordinarily good photometric stability*. There are a number of possible causes for the observed small fluctuations, including changes in the telescope point spread function, variations in the pointing during the observation, and small flux errors introduced by the resampling algorithm. Future analysis will consider available information on the JWST wavefront error and pointing stability to see if these are correlated with any changes observed in the throughput, although our preliminary estimates suggest that these were not the dominant effects for the period considered here.

As the Cycles 1 and 2 version of this monitor only checked one grating and filter combination which covers only part of the NIRSpec wavelength range, it might have missed changes that are only significant at much shorter or longer wavelengths. To put some limits on repeatability of other modes and over a broader wavelength range, we will therefore need to turn to other data. Note that while the JWST MIRI instrument did initially show significant time dependent sensitivity degradation that increased towards longer wavelengths, (see Gordon et al. 2025 and Law et al. 2025), there does not appear to have been any significant changes in the shortest wavelength MIRI bands at or below  $\sim 7$  microns, and so the systematic changes found for MIRI throughputs at longer wavelengths seem to be caused by elements of the MIRI optics (and not the OTE)..

### 3.2 Repeatability measured using other observations of flux standards.

As part of the JWST cross instrument flux measurement programs, one star is selected for each instrument to be observed annually in a wide variety of modes. For NIRSpec, this star is the solar analogue GSPC P330-E, (G1V,  $K = 11.379$ ). The NIRSpec observations of this target are listed in

Table 2. Note that this report only considers data collected through August of 2024. Later data will be discussed in a future report.

There are also several flux standards that were observed multiple times with the NIRSpec PRISM in the S1600A1 using the SUB512 aperture. These observations will be discussed in section 3.2.2, while the repeatability of P330-E grating observations with the IFU mode are presented in section 3.2.3.

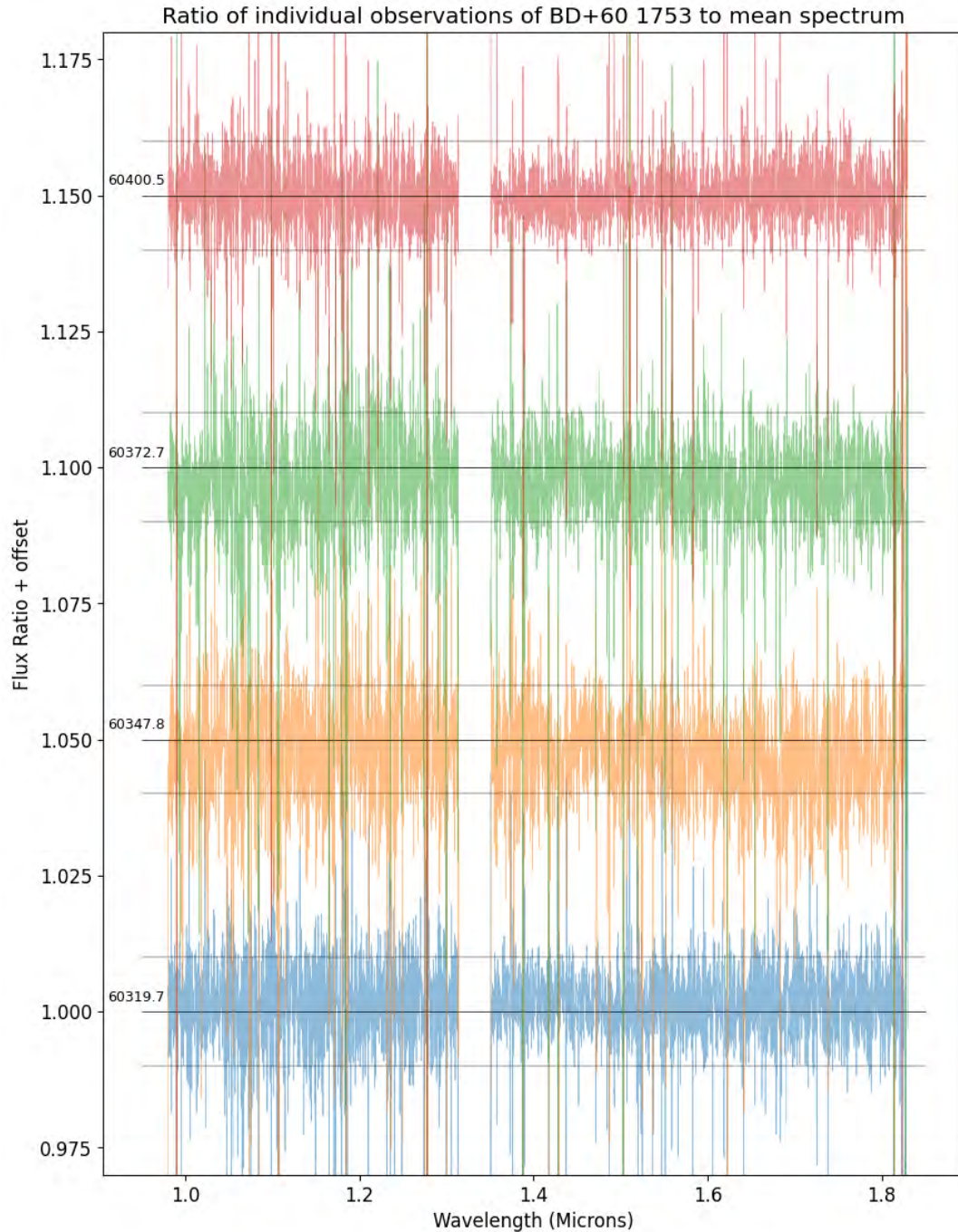


**Figure 5:** The pixel-by-pixel ratio of four of the individual G140H/F100LP observations of BD+60 1753 to the mean of all the spectra is shown. The ratios are labeled by observation date (MJD) and each is offset from the previous one by 0.05. To aid in visualizing the fluctuations around the mean, the unit ratio for each offset is marked by a bold solid line and the  $\pm 0.01$  levels are marked by thinner lines.

**Table 2: NIRSpec fixed slit observations of the solar analogue GSPC P330-E. Only observations taken on or before Aug 5 2024 are considered in this report.**

Filter/Grating	Cycle 1 – PID 1538	Cycle 2 – PID 4498	Cycle 3 – PID 6606
Fixed slit, SUB2048 NRSRAPID exposures			
G140M/F070LP	obs 160, 30-Aug-22	obs 16, 02-Jun-24	obs 31 05-Aug-24
G140M/F100LP	...	...	...
G235M/F170LP	...	...	...
G395M/F290LP	...	...	...
G140H/F070LP	...	...	...
G140H/F100LP	...	...	...
G235H/F170LP	...	...	...
G395H/F290LP	...	...	...
Fixed slit, Full-frame NRSIRS2RAPID exposures			
G140H/F100LP	obs 161, 30-Aug-22	obs 17 04/-Jun-24	not observed
G235H/F170LP	...	...	...
G395H/F290LP	...	...	...
Fixed slit, ALLSLITS NRSRAPID exposures			
G140H/F100LP	not observed	not observed	obs 32, 3-Mar-25, analysis pending
G235H/F170LP	...	...	...
G395H/F290LP	...	...	...
Fixed slit, SUB512 NRSRAPID exposures			
PRISM/CLEAR	obs 107, 30-Aug-22	obs 15 26-May/24	obs 30, 3-Mar-25, analysis pending
IFU, Full-Frame NRSIRS2RAPID exposures			
G140M/F100LP	obs 62, 07-Aug-22	obs 18, 04-Jun-24	obs 33, 3-Mar-25, analysis pending
G235M/F170LP	...	...	...
G395M/F290LP	...	...	...
G140H/F100LP	...	...	...
G235H/F170LP	...	...	...
G395H/F290LP	...	...	...

### 3.2.1 Results for P330E grating observations

All observations of P330-E done in the S1600A1 aperture used a five-point nodding pattern. We will first consider the grating observations that used the SUB2048 subarray with NRSRAPID readout.

As we did for the sensitivity monitor target, we omit any background subtraction and use only the central three dither positions for this initial comparison. We can again justify our neglect of the sky background by looking at the ETC predictions for the relative background and source count

rates for this source, but for this target we also have other observations with the high dispersion settings that were taken using full frame readouts which cover the footprints of all the NIRSpec fixed slits. Examination of these full frame rate files confirms that any sky background seen in the other slits is insignificant relative to the source flux in the S1600A1.

For these SUB2048 grating observations,

Figure 6 shows the ratio of the Cycle 2 and 3 NIRSpec observations of the solar analogue GSPC P330-E to the Cycle 1 observations of the same target with exactly the same exposure settings. In each case, the extracted cycle 2 or cycle 3 spectral flux is interpolated to the wavelength scale of the corresponding cycle 1 observation and then divided by the cycle 1 extracted spectral flux. The first panel in **Error! Reference source not found.** shows the same result for the ratio of the PID 4498 to PID 1538 observations taken using NRSIRS2RAPID with FULL frame readouts. The FULL frame IRS2 readout patterns insert extra reference pixel measurements to reduce 1/f noise, and this may explain why some of the SUB2048 observations done with the traditional NRSRAPID readout which lacks these extra reference pixels show substantially higher pixel-to-pixel variations than do the full frame observations done with NRSIRS2RAPID.

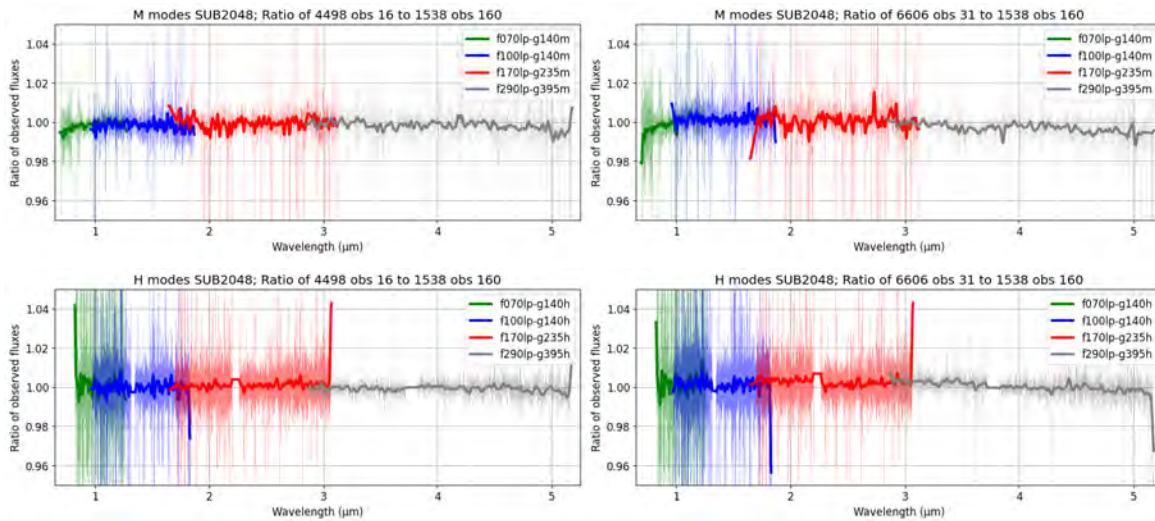


**Figure 6:** In the left-hand figures, the thin lines show the ratio of each SUB2048 exposure of P330-E from PID 4498 in June 2024 to the corresponding observation from PID 1538 obs 161 in August 2022. The thicker lines show a smoothed version of these ratios. The right-hand figures make the same comparisons for exposures from Obs 31 of PID 6606 taken in August of 2024. The upper (lower) panels show the results for the medium (high) dispersion gratings.

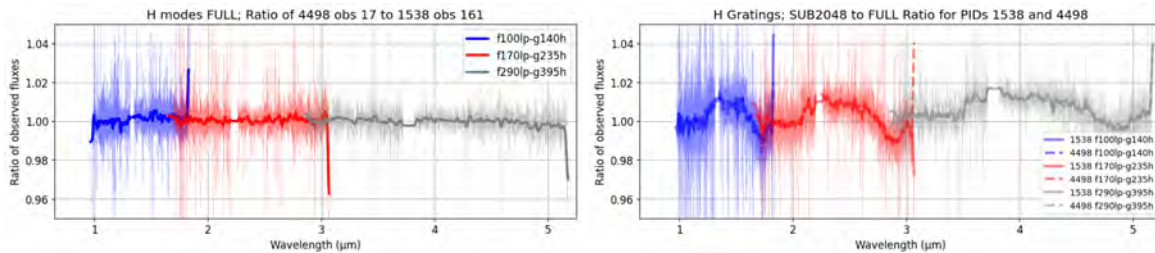


**Figure 7** The left figure shows the ratio of each FULL frame NRSIRS2RAPID observation of P330-E from PID 4498 to that from 1538 using the same conventions as in Figure 7. The right-hand figure shows the ratios of the

**SUB2048 to FULL frame observations at each of the two epochs. Note that the full frame NRSIRS2RAPID observations did not include exposures using the F070LP filter.**

To look for systematic trends that might be hidden in the small-scale pixel-to-pixel variations, we also overplot smoothed versions of the flux ratios. This smoothing is done using a three pole Bessel filter after rejecting any outliers where the ratio deviates by more than 0.1 from unity. A 27 pixel smoothing width is used for the H modes, and a 10 pixel width for the M modes, so that the smoothing kernels are approximately equivalent in wavelength.

For the G140H/F100LP setting that was used for the sensitivity monitor, changes for P330-E are also very small, consistent with the less than 0.2% rms broadband variability discussed above for BD+60 1753. Some other settings show some hints of slightly larger changes. For example, below 1 micron the 2024 and 2025 G140M/F070LP observations show a very small downward trend in measured flux relative to the 2022 observations, (see the upper panels of

Figure 6), with a maximum deviation in the smoothed spectrum of about  $-0.6\%$  near 0.7 micron. (These changes are below the minimum wavelength covered by the BD+60 1753 monitor). Also, the most recent G395M/F290LP flux measurements are perhaps 0.4% to 0.5% below the observations at the earliest epoch, but this is comparable to the maximum changes seen in the BD+60 1753 exposures.

The right-hand panel in **Error! Reference source not found.** shows the ratio of the SUB2048 NRSRAPID to full frame NRSIRS2RAPID observations at each of the two epochs at which the FULL frame data was taken. In this case, there are clear systematic differences between the readout patterns of about  $\pm 1\%$  that are very similar at both epochs and which also show very similar trends vs pixel position in all three high dispersion gratings. This suggests that there is a small issue with one of the detector-based calibrations. This could be related to the different handling of the reference pixels between the normal and IRS2 readouts, but it could also be due to differences in the linearity correction for full frame vs subarray data. NIRSpec subarray observations use a different gain setting that allows a larger range of electron signals to be measured, and this required that different external lamp exposure be used to independently measure the linearity corrections for full-frame and subarray exposures. If this is the correct explanation, we might also expect similar small offsets in the flux measurements at different exposure levels in the same setting. This could be tested by comparing the flux per read for different groups in the ramp.

Because the ratio of full-frame NRSIRS2RAPID to SUB2048 NRSRAPID observations appears to be essentially identical for both the Cycle 1 and Cycle 2 iterations, for Cycle 3 we replaced these with ALLSLITS NRSRAPID exposures to test for differences between different sized subarrays. However, these observations occurred several months after the corresponding SUB2048 observations from PID 6606, and analysis of these exposures will be discussed in a subsequent report that considers all repeated observations taken in 2025.

We also redid the above comparisons for the P330-E observations using all five dither positions with pixel-by-pixel background subtraction enabled, although to minimize the overlap of the source spectrum into the background region immediately adjacent dithers were not used as backgrounds for each other. As might be expected when averaging more exposures, the pixel-to-pixel noise was reduced in most cases, but some additional random variability in the zero-points at a level of 0.2 to 0.4% was seen. (We do not include here a separate figure to illustrate this). We suspect that vignetting near the edges of the s-flats may cause some additional uncertainty in the extracted fluxes for dither positions close to the aperture edge, as the point source spectrum

vignetting may differ slightly from that appropriate for the full aperture lamp spectra used to derive those calibration files, and the s-flat correction will be sensitive to the exact source placement.

### 3.2.2 PRISM observation repeatability in the S1600A1

In Table 3 we list, and in Figure 8 we compare, the results for all flux standards that had been observed multiple times with the NIRSpec PRISM in the S1600A1 using NRSRAPID readouts with the SUB512 subarray as of August 2024. In each case we simply interpolate the extracted spectrum of the later observation to the wavelength scale of the earlier one and divide. For J1808347 and P330E we show the ratio of the two later time observations to each other as well as the ratio of each of those to the earliest.

For this comparison, we make a few changes from the default pipeline analysis and perform some additional analysis to estimate some expected uncertainties.

Because of its low dispersion and rapid changes in throughput with wavelength, the PRISM flux extraction will be significantly more sensitive than the grating configurations to small errors in the target positioning along the dispersion direction. We simulated the effect of such a dispersion direction error by redoing the extraction of one of the spectra with the XOFFSET keyword in the input rate files set to  $-0.02$  to simulate a 20 mas error in the target location; (this value matches the nominal error budget allowed after performing a WATA TA to center the target; see <https://jwst-docs.stsci.edu/jwst-near-infrared-spectrograph/nirspec-operations/nirspec-target-acquisition/nirspec-wide-aperture-target-acquisition>). In the upper panel of Figure 9, we show the ratio of the flux from this altered spectral extraction to the nominal one.

**Table 3: Repeated PRISM observations of flux standards in the S1600A1 aperture. All used the SUB512 subarray, except for 6604/002 which used SUB2048. Note that for the PID 1487 and 4460 observations, dither positions that included offsets along the dispersion direction were excluded from the analysis to make them more comparable to the 1128 observation, and this is accounted for in the listed exposure times.**

Target	PID / Obs. No.	DATE-OBS	Groups/Ints	Dither pattern
2MASS J18083474+6927286	1128 / 005	2022-06-15	30 / 8	3 NONE
...	1487 / 012	2023-07-06	30 / 8	3 SPECTRAL
...	4460 / 012	2024-02-18	30 / 8	3 SPECTRAL
G191 B2B	1537 / 006	2022-09-25	6 / 100	5 NONE
...	1537 / 009	2022-09-25	20 / 50	5 NONE
GSPC P330-E	1538 / 107	2022-08-30	4 / 50	5 NONE
...	4498 / 015	2024-05-07	4 / 50	5 NONE
2MASS J17571324+6703409	1536 / 006	2022-08-09	5 / 30	5 NONE
...	4496 / 019	2024-05-19	5 / 20	5 NONE

There was an update to the operational SIAF file that was used for observations taken on or after 21-Sep-2022. This was accompanied by an update to the full set of instrument model files, (fpa, fore, ote, msa, collimator, camera, and disperser file types). For the S1600A1 aperture, the reference point shifted by  $+0.040''$  in V2 and  $-0.021''$  in V3 which corresponds to about  $+0.0163''$  along the NIRSpec dispersion direction and  $+0.0426''$  perpendicular to it. However, this change mostly reflects a shift in the overall alignment of NIRSpec with respect to the fine guidance sensors,

and the actual difference in the detector location at which the target acquisition places the target is typically only 0.01 to 0.02 pixels in each axis.

While the DMS pipeline always uses the latest operational SIAF to reduce all data regardless of the SIAF in effect at the time of the observation, the instrument model files used are those that were in use at the time of the observation. This introduces the possibility of a small alignment offset due to the inconsistency between the reference point locations assumed by the SIAF and the instrument model. In addition, the new instrument model files may result in a slightly different, and presumably improved, dispersion relation. In the lower panel of Figure 9 we compare the impact of using the updated instrument model files vs those in effect at the time of the observations. Given the very small offset expected for the projection onto the detector along the dispersion direction of targets located in the S1600A1, for the results we present in Figure 8, we reduced the PRISM observations taken before 21-Sep-2022 with the newer instrument model files rather than the older ones that the pipeline defaults to using. This should remove any spurious wavelength shifts due to the change in the instrument model, and seems to slightly improve the repeatability of observations taken across the SIAF update. It is expected that similar changes due to the instrument model update would be significantly smaller for the grating settings, and this was directly verified for G140M/F070LP.

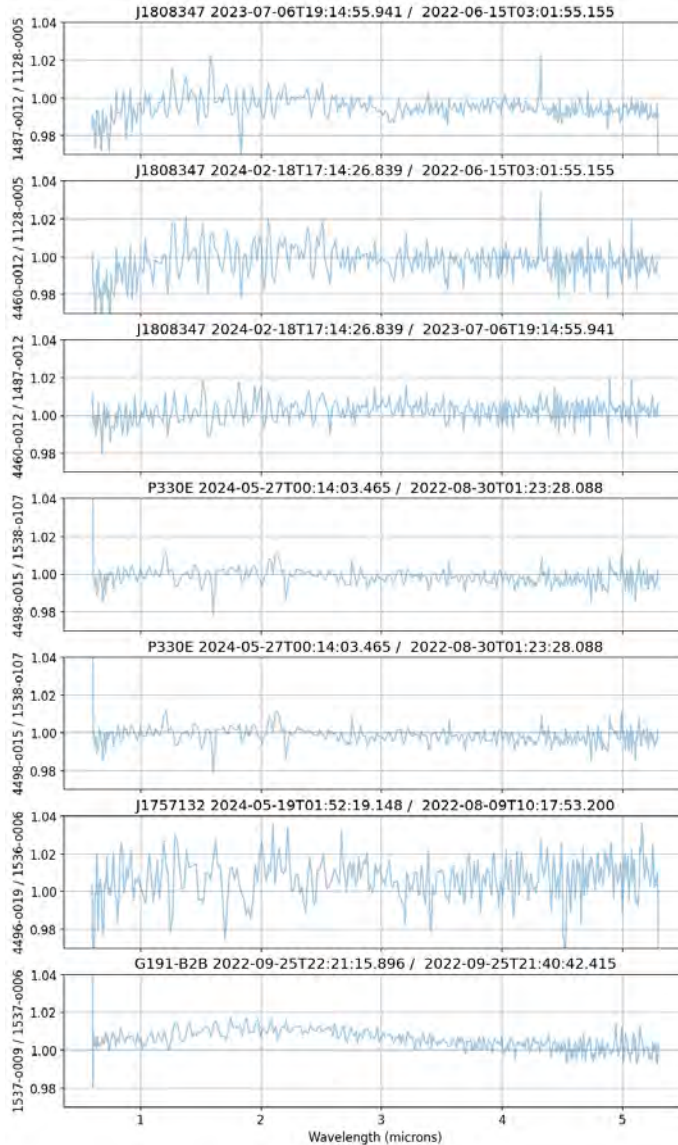


**Figure 8: For targets observed more than once with the PRISM in the S1600A1, we show the ratio of each pair of observations of the same target, in each case showing the ratio of the later to the earlier observation.**

In Figure 8, each panel shows the flux ratio, (later observation / earlier observation), as measured from duplicate PRISM observations of a given target. Several of these ratios show an  $\sim 1\%$  drop at the shortest wavelengths below 1 micron, but this primarily affects cases where the earlier exposure was taken in 2022. Reducing the data taken before the 21-Sep-2022 SIAF change with the older default instrument model files makes this discrepancy slightly but noticeably larger and adds additional smaller offsets at longer wavelengths.

There are a few additional notes for individual PRISM observations that may affect the interpretation of results.

The J1808347 observations were done with a 3 point dither pattern, while a 5 point dither pattern used for most of the other targets. The J1808347 observations in PIDs 1487 and 4460 also included some dithers in the dispersion direction, but these were excluded when producing the products

used for this analysis, so that the newer data could be directly compared to the earlier PID 1128 observations.

While the two G191 B2B observations were taken very close in time, obs 9 of PID 1537 was actually intended to observe a different, fainter, star, but instead reobserved G191 B2B due to an APT error, and, as a result, the target acquisition exposure in obs 9 was saturated and more groups were taken in each integration of obs 9 relative to obs 6.

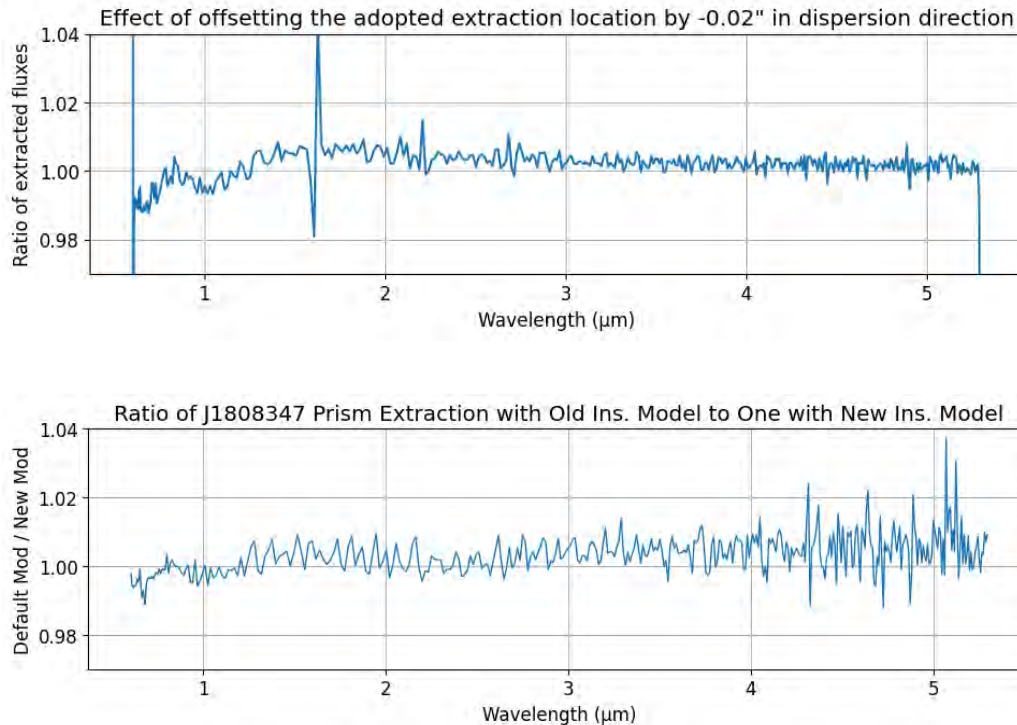


**Figure 9:** In the upper panel, we estimate the effect of pointing uncertainties in the dispersion direction by calibrating and extracting the same observation, (PID 4498 Obs 15 targeting P330-E in this case), with both the default header keywords and then again with the XOFFSET keyword offset by  $-0.02''$ , (equal to 0.2 pixels), to simulate a 20 mas misalignment after the target acquisition. This figure shows the ratio of the mis-aligned flux extraction to the nominal one. In the lower panel, we show, for observation 5 of PID 1128, the ratio of the extracted flux when using the default instrument model files used before the 21-Sep-2022 SIAF update to the flux obtained when instead using the latest instrument model files that are compatible with the later SIAF used for DMS processing.

While the biggest changes are of the same order as expected for a 20 mas offset in the target location, in practice most of the observations considered here have a signal-to-noise considerably greater than the recommended minimum of 20:1 and have a centering accuracy significantly better than the minimum requirement. We can estimate the quality of the centering by looking at the residual offset from the aperture reference point as measured in the post-TA slew reference images, and this mean residual offset along the dispersion direction for the observations considered here is  $0.005 \pm 0.026$  pixels, with the largest offset being only 0.072 pixels.

The data considered here are too sparse to conclude that the small changes at the shortest wavelengths includes any systematic trend, but, whether due to small pointing errors, alignment changes, or actual changes in throughput, it appears that observers may expect  $\lesssim 1\%$  changes in the flux measured with the NIRSpec PRISM, even for repeats of otherwise identical observations.

### 3.2.3 IFU repeatability of P330E

The flux of individual IFU exposures can vary slightly depending on the position of the target within an individual IFU slice. This effect was quantified by Pirzkal 2023 (Private communication, report on CAP 22). He found variations of up to  $\pm 4\%$  below 2.5 microns and up to  $\pm 2\%$  at longer wavelengths. For evaluating the long-term flux variability of the IFU, the best existing data are observations of P330-E from programs 1538 (obs 62 in August 2022) and 4498 (obs 18 in June 2024), which observed six of the grating settings using a standard 4 point nodding pattern. The F070LP filter settings were not included, nor was the PRISM. There was a significant change in the SIAF positioning between these two programs, and so we do not expect that the same centering within an IFU slice, and the exact regions of the detectors illuminated will have changed as well. However, many GO programs skip NIRSPEC target acquisition for IFU observations, relying only on the initial pointing accuracy, and so this may better reflect typical observations than would an exact repeat of the same pointing. Note that these IFU observations have now been repeated again in program 6606 obs 33. Comparison of those data with PID 4498 obs 18 should provide better information on the limiting precision of IFU repeatability than the existing data, but that analysis is still pending.

In Figure 10, we show the ratio of the extracted flux from each IFU set of exposures taken in June 2024 to the equivalent exposure taken in August 2022. Results presented here are Level 3 products for the merged x1d spectrum computed using the default IFU pipeline settings for JWST CALVER 1.15.1 with context `jwst_1274.pmap`. Averaging over the four nod positions is expected to average over the pathloss variations at an individual dither position. The  $\sim 1\%$  variations in the smoothed spectra seen at the shortest and longest wavelengths are consistent with the expected pathloss variations and suggest that there has been no significant change in the overall NIRSPEC IFU throughput over this period.

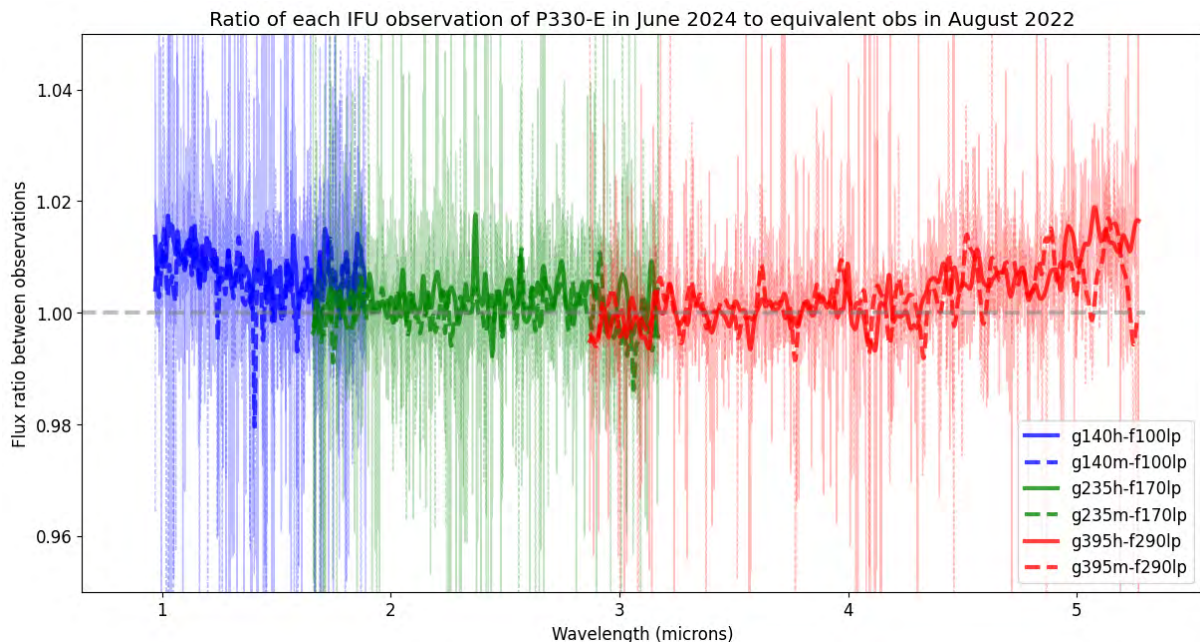


**Figure 10:** The repeatability of IFU observations of P330E is shown. The thin lines show the results of interpolating each exposure from June 2024 to the exact wavelength scale of the corresponding exposure from August 2022 and computing the ratio of extracted fluxes. The thicker lines show the result of applying a low pass filter to these ratios, using a smoothing length of 27 pixels for the high dispersion observations and 10 for the medium resolution.

## 4 Summary and Conclusions

For repeated observations of the same target with identical exposure sequences, the most extensive available data set shows that broadband flux measurements with NIRSpec can be repeated with a typical rms variability of about 0.2%. This suggests that the NIRSpec detectors and the JWST+NIRSpec optical throughput were extraordinarily stable and do not show any clear evidence for significant long term throughput changes over the period considered here.

While there is some suggestion from both the PRISM and the G140M/F070LP settings, of a slightly larger 0.5% – 1% throughput decline between mid-2022 and mid-2024 at wavelengths below 1 micron, the current data are not adequate to confirm this, as the PRISM is especially sensitive to small alignment shifts, while for the G140M/F070LP most of the effect comes from the first observation being a bit low at the short wavelength end when compared to the later two. And at the longest NIRSpec wavelengths, the more limited data available would appear to exclude changes over the same two-year period larger than about 0.5%. One caveat is that, apart from the IFU observations briefly discussed above, the bulk of this analysis has focused on the S1600A1, and so it is possible that data taken using other apertures may show larger variations, especially as the throughput of these smaller apertures will be expected to be much more sensitive to small alignment errors or PSF changes.

The IFU observations of GSPC P330E show some systematic changes of about 1% between the two epochs observed, but as there was a significant change in pointing between the two epochs, at least this level of change is expected.

In practice, the level of precision achievable for most science exposures will often not be as good as the broadband repeatability discussed above. Differences in target location within the aperture, differences between dither patterns, and errors in the linearity correction will in practice make it difficult to push relative flux comparisons between different targets below the 1 to 2% accuracy level. In addition, the flux standards which were used to define the absolute calibrations are expected to have uncertainties themselves at the 2% level, and the selection of available standards varies between modes. Observations of multiple standards in each mode will allow us to reduce the impact of this latter issue, but those observations and their analysis are still ongoing.

In summary, we conclude that the stability of the optical throughput and detector sensitivity do not appear to have been limiting factors for the NIRSpec flux accuracy over the first two years of operation.

## 5 References

- Bohlin, R. C., Gordon, K. D., & Tremblay, P.-E. 2014, *PASP*, 126, 711  
Bohlin, R. C., Krick, J. E., Gordon, K. D., et al. 2022, *AJ*, 164, 10  
Gordon, K. D., Bohlin, R., Sloan, G. C., et al. 2022, *AJ* 163, 267  
Gordon, K. D., Sloan, G. C., Garcia Marin, M., et al. 2025, *AJ* 169, 6  
Law, D. R., Argyriou, I., Gordon, K. D., et al. 2025, *AJ*, 169, 67

## Appendix A. BD+60 1753 Pointing Issues and Analysis

BD+60 1753 is too bright for a direct target acquisition with NIRSpec, and the star 2MASS J17244630+6025483 (K=13.694) at a separation of approximately 44.3" was used for an offset target acquisition. Unfortunately, the initial version of this proposal used the epoch 2000 2MASS coordinates for this offset star without any proper motion correction, and, as the actual proper motion is about 16.8 mas/yr, this resulted in BD+60 1753 being significantly offset in the aperture. While spectra were obtained, the mis-centering was enough to affect the flux at level of a couple of percent. The coordinates and proper motion of this offset star were updated to use Gaia DR3 coordinates and proper motions starting with observation 41 of PID 1539 in March 2023, and we will use only this and subsequent observations for our analysis here.

However, despite updating the coordinates and proper motion, the centering accuracy and repeatability obtained is less than desired. In part this may be because, in Gaia DR3 BD+60 1753 has an entry in the Gaia DR3 Part 3 "Non-single stars" in the table [I/357/acc7](#), "Non-single-star astrometric models for sources having a non-linear proper motion which is compatible with an acceleration solution, Acceleration model with 7 parameters". That is, the star appears to be a binary, and as such, isn't moving in a straight line. However, no orbital solution or estimate of the period is available.

If we look at the other G140H/F100LP fixed slit observations of bright standards taken observed in the S1600A1 aperture using the SUB2048 subarray after a direct target acquisition and apply the same centering algorithm used for the monitoring target, and combine the middle three dithers, we find a mean cross-dispersion centroid for the rectified spectra in the resulting S2D file of 14.05 +/- 0.05 pixels. The location of the BD+60 1753 spectra falls consistently below this by about a full pixel on average, (see Figure 11 and Figure 12). This cannot be a simple pointing error, as for a fixed error in coordinates, we'd expect the sign of the offset to change with the orient angle. To check for a possible offset in the dispersion direction, we cross-correlated the spectra with the model offsets to determine the pixel offset as a function of time. These cross-correlations assume that the velocity of the star is constant at -27.3 km/s, and if BD+60 1753 is a binary, the velocity may vary significantly between observations, by an amount larger than the measured pixel shifts. With just the G140H spectra there is no practical way to tell the difference between a velocity change of the star and a spatial offset in the aperture. Either an orbital solution for the system from another source would be needed, or medium and high-res spectra taken in the same band would be needed at each epoch.

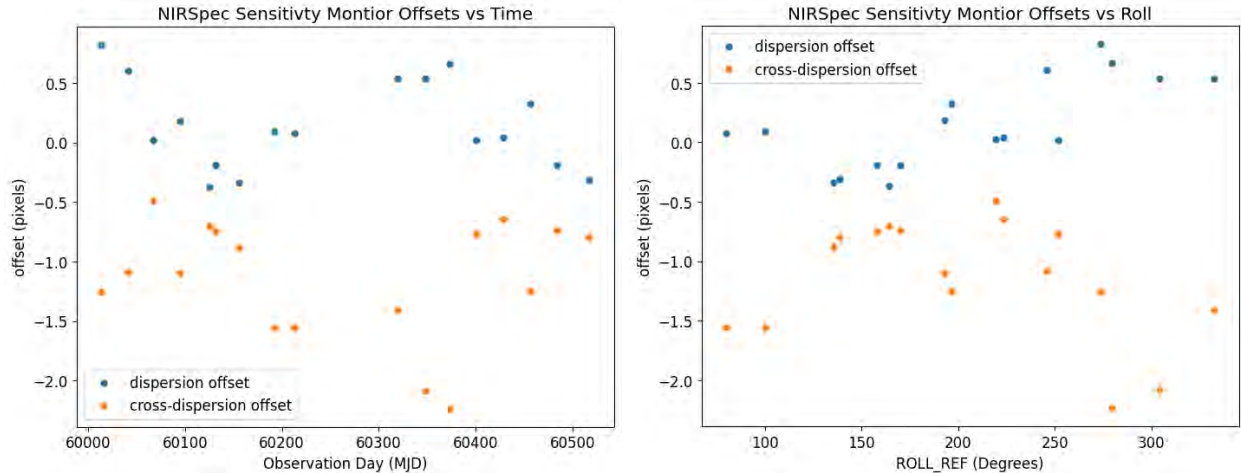


**Figure 11:** These plots show the inferred offsets of the target from the expected location in the aperture for the sensitivity monitor observations. The cross dispersion offset compares the measured centroid from the typical centroid of a similar observation done with a direct target acquisition, while the offset in the dispersion direction assumes that the target velocity is constant at the  $-27.3$  km/s value given in the calspec (Bohlin et al 2014; 2022) reference file.

Even allowing for a zero-point offset in the cross-dispersion position, the measured shifts do not seem to be compatible with a simple coordinate offset as one would expect the dispersion and cross-dispersion offsets to be 90 degrees out of phase; i.e., if one was at an extremum, the other would be near its mean value.

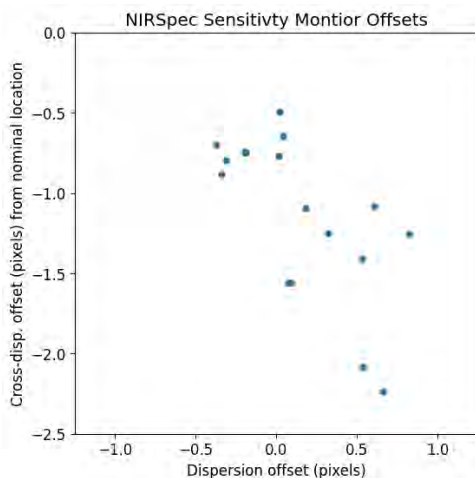


**Figure 12:** The cross-dispersion and inferred dispersion direction offsets are compared.

These offsets push the lowest of the 5 dither positions into a region where the flux calibration is severely compromised. These data appear to be affected not only by vignetting due to the aperture edge but also appear to show significant resampling errors due to edge effects in the 2D rectification algorithm. Since we were unable to come up with a clear explanation for these pointing offsets, we have used only the central three dither positions of BD+60 1753 for the main repeatability analysis.

Given the substantial history of observations already obtained with this target, we are reluctant to recommend a change to a fainter star that could be acquired without use of an offset TA target. We suggest that other observations where both the offset and science target have excellent position

information and proper motions be analyzed to exclude the possibility that there might be some small systematic error in the slew calculations and verify at least the cross-dispersion target positioning accuracy for NIRSpec as a function of offset slew length. These should be checked as a function of position on the sky, slew length, and spacecraft attitude. NIRSpec BOTs observations using the G395H grating appear to provide the most numerous candidates for such checks of offset target acquisitions, but such an analysis would need to carefully consider any errors in GO supplied offset and/or target coordinates and proper motions.